
Explosive disruption of long-term eruptive activity at Santiaguito, Guatemala

Oliver D. Lamb^{1,2*}, Anthony Lamur¹, Alejandro Díaz-Moreno¹, Silvio De Angelis¹, Adrian J. Hornby^{1,3}, Felix W. von Aulock¹, Jackie E. Kendrick¹, Paul A. Wallace¹, Andreas Rietbrock^{1,4}, Isaac Alvarez⁵, Gustavo Chigna⁶, and Yan Lavallée¹

¹*Dept. of Earth, Ocean and Ecological Sciences, University of Liverpool, Liverpool, UK*

²*Dept. of Geological Sciences, University of North Carolina at Chapel Hill, Chapel Hill, NC, USA*

³*Dept. of Earth and Environmental Sciences, Ludwig-Maximilians Universität München, Munich, Germany*

⁴*Geophysical Institute, Karlsruhe Institute of Technology, Karlsruhe, Germany*

⁵*Dept. of Signal Theory, Telematics and Communications, University of Granada, Granada, Spain*

⁶*Instituto Nacional de Sismología, Vulcanología, Meteorología, e Hidrología (INSIVUMEH), Guatemala City, Guatemala*

Correspondence*:

Oliver D. Lamb, Dept. of Geological Sciences, 104 South Road, Mitchell Hall, Chapel Hill, NC, 27599-3315 USA
olamb@email.unc.edu

2 ABSTRACT

3 A comprehensive understanding of the dynamic evolution of active volcanic systems requires
4 extensive sets of geophysical and geological data to fully constrain and understand shifts in
5 eruptive behavior. The Santiaguito dome complex, Guatemala, is a remarkable example of an
6 open-vent volcanic system where continuous eruptive activity has historically been characterized
7 by cycles of effusion and frequent, small to moderate, gas-and-ash explosions. During 2015-2016
8 the volcano experienced a rapid intensification of activity including large vulcanian explosions,
9 frequently accompanied by pyroclastic density currents. Here we present a chronology of the
10 eruptive activity at Santiaguito from November 2014 - May 2017, compiled from field observations
11 (visual and thermal) and activity reports. We also present seismic and acoustic infrasound data
12 collected during the same period, the longest and largest dataset collected at Santiaguito to date.
13 Three major phases of eruptive activity took place during the study period. The first phase was
14 consistent with the long-term eruptive behavior reported at Santiaguito by previous studies: lava
15 effusion simultaneous with small (<1 km plume height), regular (25-200 minute intervals), gas-
16 and-ash explosions. The second phase from July 2015 to September 2016 was defined by large
17 (<5-7 km plume height) vulcanian explosions at irregular intervals and often accompanied by
18 pyroclastic density currents. The third phase was marked by a return to effusive activity in October
19 2016 interspersed by small, gas-rich explosions. Over 6000 explosive events were recorded by
20 seismic and infrasound during the study period and clearly delineate the three phases of activity

21 at the volcano. The data presented here also include the first documented geophysical evidence
22 of explosion blast waves and volcano-tectonic earthquake swarms at Santiaguito. The dataset
23 introduced here will serve as the foundation for future studies of the long-lived effusive eruption
24 and rapid transitions to explosive volcanic activity at Santiaguito dome complex.

25 **Keywords:** Santiaguito, volcano-seismology, infrasound, eruption chronology, volcanic explosions, thermal images

1 INTRODUCTION

26 Lava dome eruptions are characterized by the slow extrusion of highly viscous, degassed magma that
27 accumulates on or near a vent and can eventually form voluminous edifices ($>1 \text{ km}^3$; Fink, 1990). They
28 are found across a range of tectonic settings and commonly develop at stratovolcanoes as well as along
29 extensive fissures (Fink, 1990). These eruptions occur over a wide range of timescales, from months
30 to decades, and often involve multiple episodes of explosive activity and/or collapses which commonly
31 produce hazardous pyroclastic density currents (PDCs; Calder et al., 2015).

32 Shifts in eruptive behavior at active lava domes present a significant challenge for monitoring and hazard
33 assessment, particularly as transitions from effusive to explosive activity, and vice versa, can be rapid
34 (e.g. Surono et al., 2012) and often lack obvious geophysical precursors (e.g. Reyes-Dávila et al., 2016).
35 Pressurization, due to gas fluxing (e.g. Michaut et al., 2013; Johnson et al., 1998) or fresh magma recharge
36 (e.g. Reyes-Dávila et al., 2016), may trigger explosive activity and evolution in associated monitored
37 signals (Sparks, 1997). Generally, the switch from effusive to explosive activity during lava dome eruptions
38 have been characterized by variations in magma discharge rate (Sparks, 1997) and volcano-seismic activity
39 associated with magmatic or fluid movement (e.g. Neuberg, 2000; Arámbula-Mendoza et al., 2011). It is
40 commonly believed that the competition between gas pressure and the rheology of dome lavas controls the
41 development of fractures (Lavallée et al., 2008; Scheu et al., 2008; Heap et al., 2015a), porosity (Heap et al.,
42 2015b; Rhodes et al., 2018) and coherence (e.g. Tuffisites; Kendrick et al., 2016), and thus permeability
43 (Scheu et al., 2008; Lavallée et al., 2013; Gaunt et al., 2014; Farquharson et al., 2015), leading to either
44 fragmentation and explosive activity (e.g. Dingwell, 1996; Papale, 1999) or outgassing and effusive activity
45 (e.g. Edmonds et al., 2003; Gonnermann and Manga, 2007). To understand the relationships between
46 these key characteristic signals, long-term investigations using multi-parameter datasets are of particular
47 value. Such investigations have become a strategic requirement for the development of more sophisticated
48 models that integrate the spectrum of magmatic processes governing lava dome activity (e.g. Soufrière
49 Hills volcano; Wadge et al., 2014).

50 The Santiaguito dome complex in Guatemala is a rare example of a long-term lava dome eruption
51 that has experienced multiple transitions between effusive and explosive activity (Harris et al., 2003;
52 Rhodes et al., 2018). From November 2014 to May 2017, the University of Liverpool and the Instituto
53 Nacional de Sismología, Vulcanología, Meteorología, e Hidrología (INSIVUMEH), deployed a network
54 of seismometers and infrasound microphones around Santiaguito. The deployment was complemented
55 by thermal and optical records of activity recorded during multiple field campaigns. The investigation
56 was motivated by the need to characterize the activity and understand long-term eruptive behavior at the
57 volcano. Serendipitously, our study covered a period of paroxysmal activity between late 2015 and mid
58 2016. Here, we present a review of geophysical data and field observations recorded during a long-term,
59 multi-parameter investigation of lava dome activity at Caliente, including the period of intense explosive
60 activity during 2015-2016.

2 SANTIAGUITO DOME COMPLEX

61 Santiaguito is a $\sim 1.1 \text{ km}^3$ active complex of lava domes located 110 km west and 11 km south of the cities
62 of Guatemala City and Quetzaltenango, respectively (Harris et al., 2003). The dome complex first began
63 extruding in 1922 into an eruption crater on the southwestern flank of Santa Maria volcano (Rose, 1973).
64 The crater formed during the October 1902 eruption of Santa Maria which deposited $\sim 8.3 \text{ km}^3$ of dacite
65 over an area of $1.2 \times 10^6 \text{ km}^2$ across Central America; one of the largest eruptions of the twentieth century
66 (Williams and Self, 1983). The dome complex has been continuously active from 1922 to the present day,
67 producing four lava domes: El Caliente, La Mitad, El Monje and El Brujo (Rose, 1973). Extrusion rates
68 have shown a distinctly cyclic nature with at least nine cycles identified with periods of 7-15 years length
69 (Harris et al., 2003; Rhodes et al., 2018). These cycles are also defined by rheological shifts that have
70 promoted different eruptive lava structures (Rhodes et al., 2018). Since 1977, activity has been focused
71 at the El Caliente vent and consists of semi-continuous extrusion of blocky lava flows interspersed by
72 frequent gas-and-ash explosions. Occasional escalations in explosive activity have included dome collapse
73 and PDCs (Rose, 1987; Harris et al., 2003). For the past two decades, explosions have generally been
74 of small to moderate size with volatile-rich, ash-poor plumes typically reaching 1-2 km above the vent
75 (Sahetapy-Engel et al., 2008; Johnson et al., 2014; De Angelis et al., 2016). Through the course of the
76 eruption since 1922, the erupted lava has become progressively less evolved with a $\sim 4 \text{ wt.}\%$ decrease in
77 bulk SiO_2 between 1922 and 2002 (Scott et al., 2013). Given the steadily decreasing extrusion rates and
78 bulk SiO_2 composition observed up to the time of writing, Harris et al. (2003) estimated that activity at
79 Santiaguito would terminate in 2014-2024. However, renewed effusive and explosive activity since 2010
80 has raised questions about magmatic processes in the source region.

81 Santiaguito has been the subject of several multi-parametric monitoring campaigns taking advantage
82 of the continuous nature of the eruption, the regular occurrence of explosive activity, and a direct view
83 into the eruptive vent from a vantage point on Santa Maria (Bluth and Rose, 2004; Johnson et al., 2004,
84 2008; Sahetapy-Engel et al., 2008; Yamamoto et al., 2008; Johnson et al., 2009; Johnson and Lees, 2010;
85 Sanderson et al., 2010; Holland et al., 2011; Johnson et al., 2011; Jones and Johnson, 2011; Johnson et al.,
86 2014; Scharff et al., 2014; Kim and Lees, 2015; Lavallée et al., 2015; De Angelis et al., 2016). Previous
87 studies have focused on volcano-seismic and infrasound signals generated during small volcanic explosions
88 (Johnson et al., 2008, 2009; Johnson and Lees, 2010). Abrupt vertical displacements of lava at or near
89 the surface of the vent immediately prior to or during explosions are thought to play a significant role in
90 generating long-period volcano-seismic signals (Johnson et al., 2008, 2009) and infrasound signals with
91 peak amplitudes of up to 5 Pa (Johnson and Lees, 2010; De Angelis et al., 2016). The regular explosions
92 at Santiaguito have presented an ideal ground for testing methods designed to accurately locate and
93 characterize explosive activity, including semblance mapping (Johnson et al., 2011; Jones and Johnson,
94 2011) and Time Reversed Migration (Kim and Lees, 2015). None of the above studies have described and
95 analyzed a dataset that spanned more than a few weeks of eruptive activity.

96 Most geophysical studies at Santiaguito have aimed to understand the trigger mechanisms for outgassing
97 vs. explosive activity during periods of dome extrusion (Sahetapy-Engel et al., 2008; Sanderson et al.,
98 2010; Holland et al., 2011; Johnson et al., 2014; Scharff et al., 2014; Lavallée et al., 2015). So far, two
99 mechanisms have been proposed to underlie the explosive activity: (1) rupture of magma in marginal shear
100 zones of the lava column, or (2) disruption of a gas-rich magma pocket at a shallow depth. The former
101 mechanism is based on a notion that the upper degassed part of the magma column ascends in a staccato
102 manner causing shear-induced fragmentation at the conduit margins (Goto, 1999; Papale, 1999). The
103 mechanism has been inferred during dome extrusion at Montserrat (Neuberg et al., 2006), the 2004-2008

104 eruption at Mount St. Helens (Iverson et al., 2006), and during spine extrusion at Unzen volcano (Goto,
105 1999; Lamb et al., 2015). In turn, this rupture mechanism produces temporary networks of shear fractures
106 near the conduit margins that drive rapid outgassing of shallow (<600 m) magma along arcuate fractures
107 (e.g. Harris et al., 2003; Johnson et al., 2008; Holland et al., 2011; Lavallée et al., 2013; Scharff et al., 2014,
108 Hornby et al. *in prep*). At Santiaguito, friction during shear failure has been shown to generate enough
109 heat to partially melt the crystal phases and induce rapid volatile exsolution from the magma, driving
110 explosions from the arcuate fractures (Lavallée et al., 2015). Tests on dome material demonstrate how these
111 arcuate fractures form through coalescence of tensile fractures generated during repeated deformation of the
112 shallow magma conduit (Hornby et al. *in prep*). The second mechanism, where a gas-rich region in the
113 magmatic column drives explosive activity, is based on modeling of a pressure source to explain the cyclic
114 deformation at Santiaguito (Sanderson et al., 2010; Johnson et al., 2014). Brief episodes of strong gas
115 emissions and explosions are commonly observed at the apex of inflation cycles, monitored by tiltmeters or
116 long period seismometers (Johnson et al., 2014). It has been noted that explosions are accompanied by
117 more pronounced inflation/deflation cycles and very long period seismicity, whereas outgassing events
118 are aseismic and accompanied by steady inflation/deflation cycles (Lavallée et al., 2015). It is likely that a
119 combination or sequence of the above mechanisms underlies regular explosive activity at Santiaguito.

120 2.1 Multi-parametric Observations

121 An intensive multi-parametric monitoring investigation was conducted at Santiaguito from November
122 2014 to May 2017, the first such long-term study of the volcano. We conducted 7 multi-parametric field
123 campaigns in November 2014, April 2015, December 2015, January 2016 (as part of the Workshop on
124 Volcanoes), June 2016, February 2017 and May 2017. In November 2014, we deployed a temporary network
125 of geophysical instruments consisting of eleven seismometers and five acoustic infrasound microphones
126 (Fig. 1). The seismometer network included five Nanometrics Trillium Compact (T=120s) three-component
127 broadband instruments, and six Lennartz LE-3Dlite (T=1s) three-component short-period instruments. The
128 microphones were iTem prs100 instruments (Delle Donne and Ripepe, 2012) and were co-located with the
129 broadband seismometers. Table 1 lists all the stations deployed in the network, along with their dates of
130 deployment and recovery. The stations were strategically deployed around the Santiaguito dome complex
131 to achieve optimal azimuthal coverage (Fig. 1). Data were recorded on-site at a rate of 100 Hz, with 24-bit
132 resolution.

133 During the visits to Santiaguito, we complemented the geophysical dataset with optical and thermal
134 observations. Thermal infrared (TIR) videos were recorded with a FLIR T450sc infrared camera equipped
135 with a 30 mm lens (FOV: 15 x 11.25, IFOV: 0.82 mrad). During thermal image capture, we recorded the
136 atmospheric temperature, humidity, and the distance from the lava dome for appropriate corrections of
137 signal transmissivity through the atmosphere.

3 ERUPTIVE ACTIVITY DURING 2014-2017

138 The following chronology is based on a combination of observations compiled by the authors during
139 multiple field campaigns from 2014-2017 and are summarized in Figure 2. We have identified three phases
140 of activity at Santiaguito, each defined by changes in eruptive activity: November 2014 - June 2015, July
141 2015 - September 2016, and October 2016 to May 2017. We also begin this section by describing the
142 significant eruptive activity which took place at Santiaguito in 2014, before commencement of the field
143 campaigns in November 2014. Further details are derived from monitoring observations at INSIVUMEH,

Station	Installed	Recovered	Seismometer	Microphone
LB01	20/11/2014	16/05/2017	Trillium T120 Compact	iTem prs100
LB02	21/11/2014	16/05/2017	Trillium T120 Compact	iTem prs100
LB03	23/11/2014	20/05/2017	Trillium T120 Compact	iTem prs100
LB04	24/11/2014	01/12/2015*	Trillium T120 Compact	iTem prs100
LB05	24/11/2014	01/12/2015*	Trillium T120 Compact	iTem prs100
LB06	15/06/2016	16/05/2017	Trillium T120 Compact	iTem prs100
LB07	16/06/2016	19/05/2017	Trillium T120 Compact	iTem prs100
LS01	19/11/2014	17/05/2017	Lennhartz LE-3Dlite	-
LS02	19/11/2014	17/05/2017	Lennhartz LE-3Dlite	-
LS03	19/11/2014	05/12/2015	Lennhartz LE-3Dlite	-
LS04	24/11/2014	18/05/2017	Lennhartz LE-3Dlite	-
LS05	27/11/2014	19/05/2017	Lennhartz LE-3Dlite	-
LS06	28/11/2014	20/05/2017	Lennhartz LE-3Dlite	-
LS07	06/12/2015	18/05/2017	Lennhartz LE-3Dlite	-

Table 1. Details of the stations deployed in the temporary network at Santiaguito dome complex. Station short-hand names are shown in first column, along with date of installation, and specific type of instruments used. ‘LB’ indicates the station used a broadband seismometer, whereas ‘LS’ used a short-period seismometer. Also indicated are stations whose equipment were removed from their original locations due to technical difficulties. ‘LB04’, ‘LB05’, and ‘LS03’ were moved to ‘LB06’, ‘LB07’, and ‘LS07’, respectively. *Stations LB04 and LB05 were inactive from Mid-December 2014 onwards, but only removed 12 months later due to inaccessibility.

144 also reported in the Bulletin of the Global Volcanism Network, available on the Global Volcanism Program
145 website (volcano.si.edu).

146 3.1 Significant 2014 activity

147 Regular activity at Santiaguito during 2014 was punctuated by a major dome collapse followed by the
148 emplacement of a lava flow. The collapse, which occurred on 9th May, removed a significant section of the
149 eastern flank of El Caliente vent and produced a PDC that traveled ~7 km to the south; approximately 1×10^6
150 m^3 of tephra was deposited. This was followed in the next two weeks by a series of lahars, including two
151 major events on 6th June and 15th July that damaged local infrastructure and forced temporary evacuations.
152 Shortly after the 9th May collapse, a lava flow was observed descending the newly formed collapse scar
153 and generating incandescent rockfalls. The flow continued for the rest of 2014, splitting into two lobes and
154 eventually halting in December at a final length of 3.5 km from the El Caliente vent (Global Volcanism
155 Program, 2015). Throughout this period of activity, small gas-and-ash explosions continued to occur at
156 regular intervals, forming plumes up to 1 km above sea level (a.s.l.). No large explosions were reported
157 during this period.

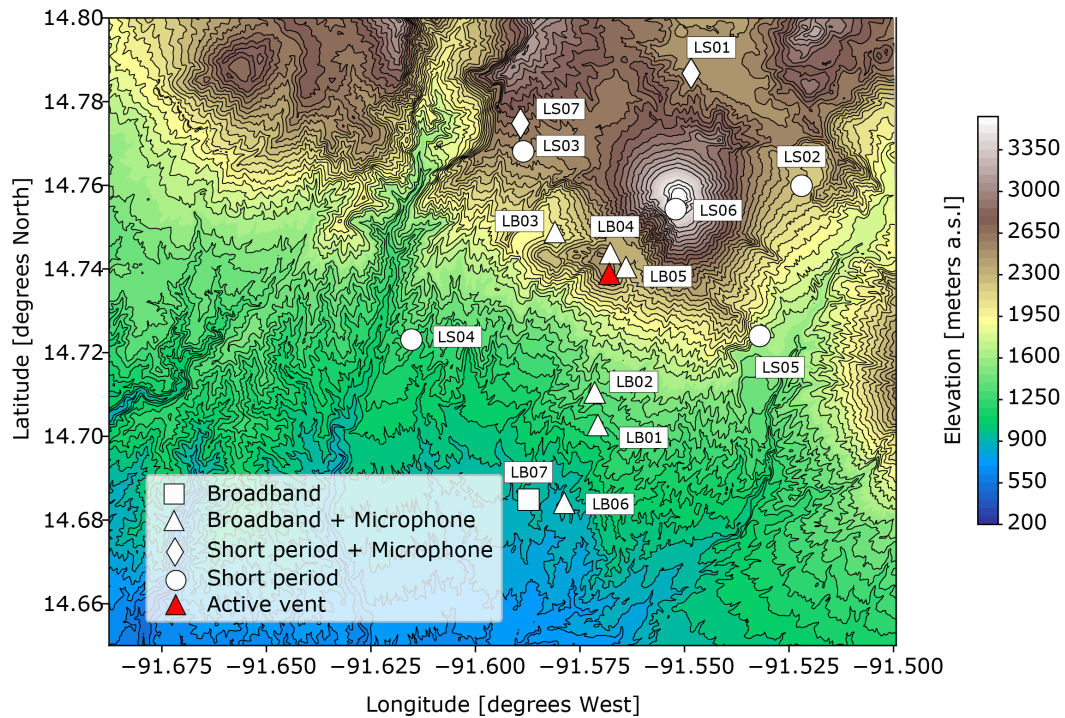


Figure 1. Map of the Santiaguito dome complex with the locations of deployed seismic and acoustic stations in the area. Red triangle marks the location of the active El Caliente vent. Station LS06 is deployed near the vantage point on Santa Maria volcano.

158 3.2 Phase 1: November 2014 - June 2015

159 During the deployment of the instrument network in November/December 2014, regular gas-and-ash
 160 explosions were observed from El Caliente (Fig. 2B). Incandescence was observed at the vent, although
 161 lava effusion was negligible or had ceased (Fig. 3A, B). Joint analysis of infrasound, thermal images and
 162 collected ash indicated that these explosions carried only minor ash fractions, suggesting that no extensive
 163 magma fragmentation was occurring in the conduit (De Angelis et al., 2016). Previous investigations
 164 have found correlations between local incandescence intensity and gas fluxing from the vent surface of El
 165 Caliente (Johnson et al., 2014). We observe a variation in the location of temperature intensities across the
 166 surface of the vent during this time period (Fig. 3A, B), indicating the dynamic nature of the vent during
 167 this phase. Frequent rockfalls occurred at the top of the lava flow on the El Caliente vent rim, and at or
 168 near the front of the lava flow lobes. Rockfalls were also frequently observed descending the unstable 1902
 169 crater wall on the southwestern flank of Santa Maria (not linked to the ongoing effusive activity). No large
 170 explosions or PDCs were reported during this period.

171 3.3 Phase 2: July 2015 - September 2016

172 Regular explosive activity continued until July/August 2015. At this point explosions were less regular
 173 (<10 per day) and more energetic than before, sometimes accompanied by PDCs (Fig. 2C). The largest
 174 group of explosions in 2015 were observed in December, producing ash plumes up to 7 km a.s.l. The
 175 explosions during this phase of activity were visually darker and thus more ash-rich than in 2014. Fine ash
 176 fell at least 10 km from the vent in all directions, and eruptive plumes were tracked by the Washington

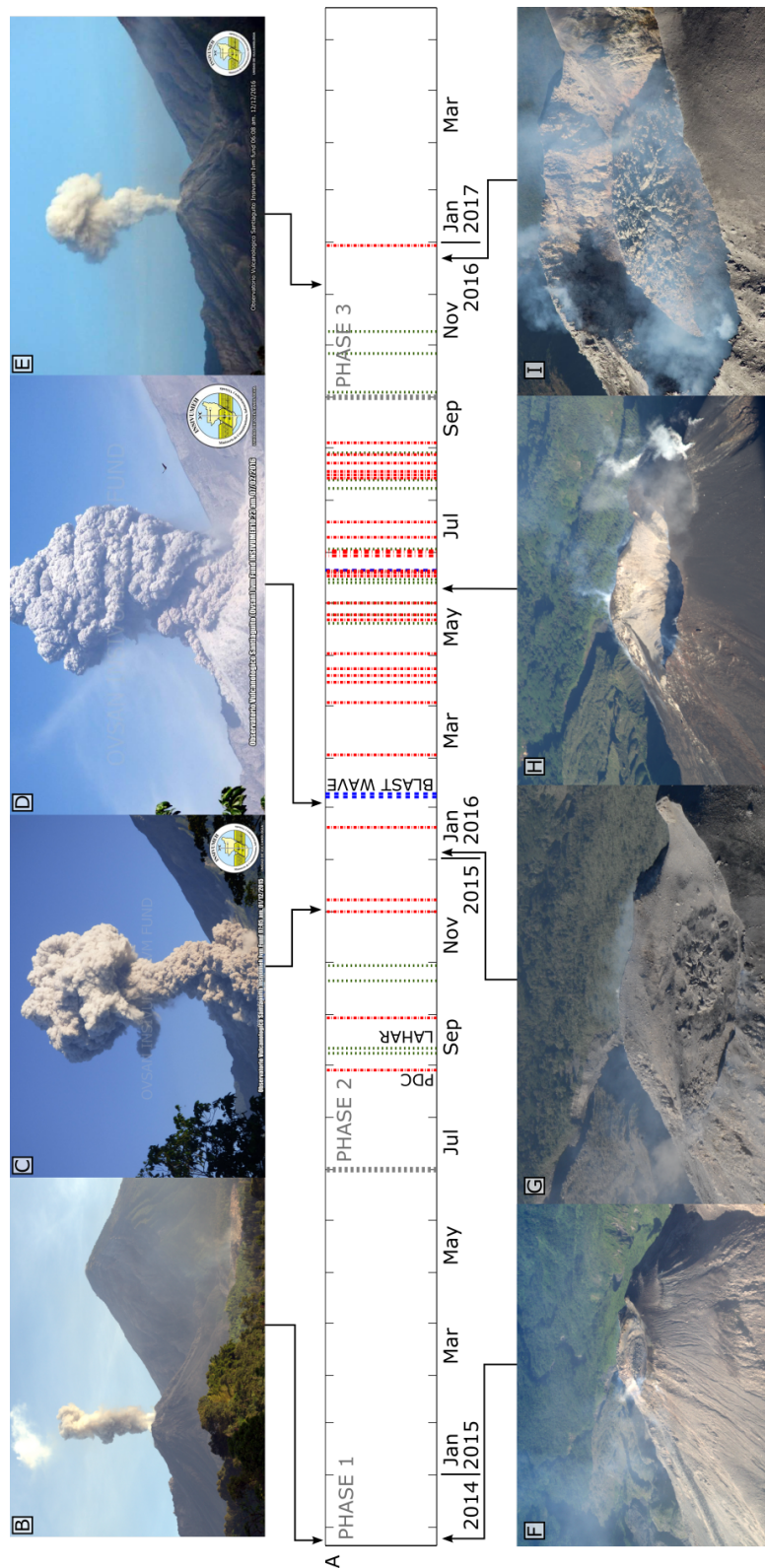


Figure 2. (A) Timeline of activity at Santiaguito dome complex between November 2014 and May 2017. Grey dashed lines separate different phases of activity. Red dashed lines indicate explosions accompanied by pyroclastic density currents (PDCs). Green dashed lines indicate reported major lahars. Blue dashed lines indicate explosions accompanied by reported blast waves. (B-E) Images of explosions during this period. Images C-E were kindly provided by INSIVUMEH. (F-I) Images of the evolution of El Caliente vent during our period of study, as seen from Santa Maria volcano. Image (I) was provided courtesy of A. Pineda.

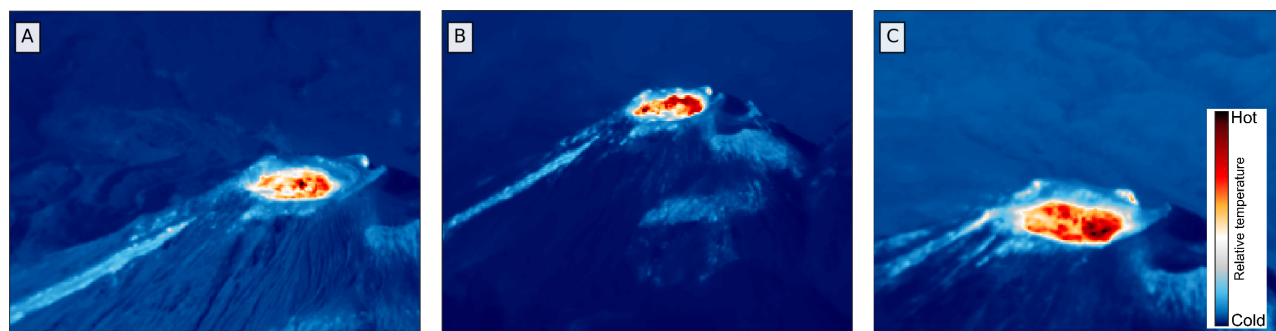


Figure 3. Composite thermal images of the El Caliente dome and vent recorded from the vantage point on Santa Maria during (A) 29/11/2014, (B) 27/03 – 03/04/2015 and (C) 07 – 09/01/2016. The images were generated by stacking the frames of thermal videos taken during these time periods, thus they represent an average of the relative dome temperature distributions during each period.

177 VAAC for 280 km before dissipating. During this phase, heavy rainfall triggered hot lahars that descended
 178 along river drainages to the south on 8th September, 11th September, 21st October and 30th October (Global
 179 Volcanism Program, 2016a).

180 From January to June 2016, major ash-rich explosions and PDCs occurred at irregular intervals with
 181 smaller explosions in between. Plumes rose to 5 km a.s.l. with ash regularly falling on villages up to 20 km
 182 from the vent. Thermal images captured in January 2016 indicate higher temperatures over a broader area
 183 of the vent surface (Fig. 3C). In February 2016, a series of strong explosions were reported to be producing
 184 dense ash clouds up to 6 km a.s.l. and accompanied by PDCs. Explosions on 7th February were heard up
 185 to 25 km away (Global Volcanism Program, 2016b). The largest explosions of the entire 2-year period,
 186 observed in April and May 2016, ejected 2 - 3 m diameter blocks up to 3 km away from the vent, and
 187 excavated the summit crater to ~300 m width and ~175 m depth (Fig. 2H). In early July, large meter-size,
 188 breadcrumb bombs were discovered ~1.8 km away from the vent (Figure S1). Heavy rainfall triggered two
 189 lahars in May, five in June, four in August, and a further ten in September (Global Volcanism Program,
 190 2016b, 2017). Irregular, large, explosions occasionally accompanied by PDCs continued through July,
 191 August, and into September.

192 3.4 Phase 3: October 2016 - May 2017

193 In October 2016, a new phase of activity was observed, characterized by the extrusion of lava into the
 194 summit crater of El Caliente (Fig. 2I). By February 2017, this new lava extrusion had filled over 60% of
 195 the summit crater. By March 2017, the extrusion had grown large enough that occasional block-and-ash
 196 flows descended tens of meters down the flanks of El Caliente. Concurrently, the number of low- to
 197 moderate-energy explosions from the El Caliente was reported to increase gradually, reaching up to 35
 198 events per day in May 2017 (Global Volcanism Program, 2017). No large vulcanian explosions were
 199 reported during this phase.

4 SEISMIC AND ACOUSTIC INFRASOUND

200 The characteristics of seismic and acoustic signals recorded by our network of instruments during 2014-
 201 2017 exhibit substantial variability. Here we provide a synopsis of key geophysical observations within

202 the context of the activity described in Section 3, and observations of past eruptive activity as reported by
203 previous studies.

204 4.1 Activity overview

205 An overview of seismic activity between November 2014 and May 2017 is provided by the network-
206 averaged Real-Time Seismic Amplitude Measurement (henceforth referred to as the Network RSAM)
207 shown in Figure 4. RSAM is a continuous measurement of the seismic intensity recorded at a station
208 and was developed to quickly assess volcanic activity (Endo and Murray, 1991). As no station operated
209 continuously throughout the whole study period, it was necessary to construct a Network RSAM, which
210 uses data from multiple stations across the network. (A detailed description of how Network RSAM was
211 generated is provided in section 1.1 of the supplementary material.) Network RSAM is generally low
212 throughout our entire period of study, although frequently punctuated by large spikes in amplitude (Fig.
213 4A). The size and frequency of these spikes increase after July 2015, the largest occurring in March 2016.
214 Most of these spikes are associated with explosive activity at Santiaguito, with some produced by tectonic
215 earthquakes within 800 km of the volcano ($M6+$, marked by red triangles in Fig. 4A), or lahars in the
216 region.

217 To follow trends in eruptive activity during our study period, we have automatically tracked the rate of
218 explosive activity at Santiaguito using the seismic and infrasound datasets. Explosive activity at Santiaguito
219 has previously been observed to frequently occur with a pulsatory nature, with multiple distinct explosions
220 occurring within a relatively short interval of time (<30 s spacing; Scharff et al., 2014; Johnson et al., 2014).
221 The distinct explosion pulses may erupt from one or more different fractures across the surface of the
222 active El Caliente vent (Jones and Johnson, 2011; Scharff et al., 2014). Here we define a single ‘explosive
223 event’ as that which includes at least one explosive pulse within a short time interval (<120 s). Seismic
224 waveforms from each event were detected using an envelope matching algorithm and cross-referenced
225 with acoustic triggers selected via a waveform characterization algorithm (Díaz-Moreno et al. *in prep*).
226 The algorithm uses infrasound waveform shape, amplitude and frequency content to search for explosion
227 waveforms and includes noise reduction techniques to amplify signals of low signal-to-noise ratio.

228 In total, 6104 explosive events were detected between November 2014 and May 2017, with large
229 variations in the number of events per day (Fig. 4B). In December 2014 and during the first half of 2015
230 (Phase 1), explosions occurred at high rates (>20 events per day) similar to activity reported in previous
231 studies and reports (e.g. Johnson et al., 2014). However, it is clear that the rate of explosive events show
232 a consistent linear decrease through the latter half of Phase 1 and into Phase 2. This indicates that the
233 transition between Phase 1 and 2 was gradual instead of sudden, as might be inferred from activity reports
234 (Section 3). Event rates between mid-2015 and the end of September 2016 (Phase 2) consistently remained
235 at low levels, with <10 events per day. This trend in activity continued until late 2016, when a 2-month
236 long period of increased rate of explosions was observed. This coincides with the beginning of effusive
237 activity that defines Phase 3. We note here that the explosion rates characterized using waveform picking in
238 late 2016 and into 2017 falls below the explosion rates presented in activity reports (Section 3.4). This may
239 be due to our definition of an ‘explosive event’, low signal-to-noise ratios or data dropouts due to technical
240 issues. Therefore, we acknowledge that this dataset likely underrepresents the true number of low-energy
241 explosions that occurred during our period of study. Nevertheless, the results plotted in Figure 4B are a
242 good indicator of the changes in activity taking place at the volcano.

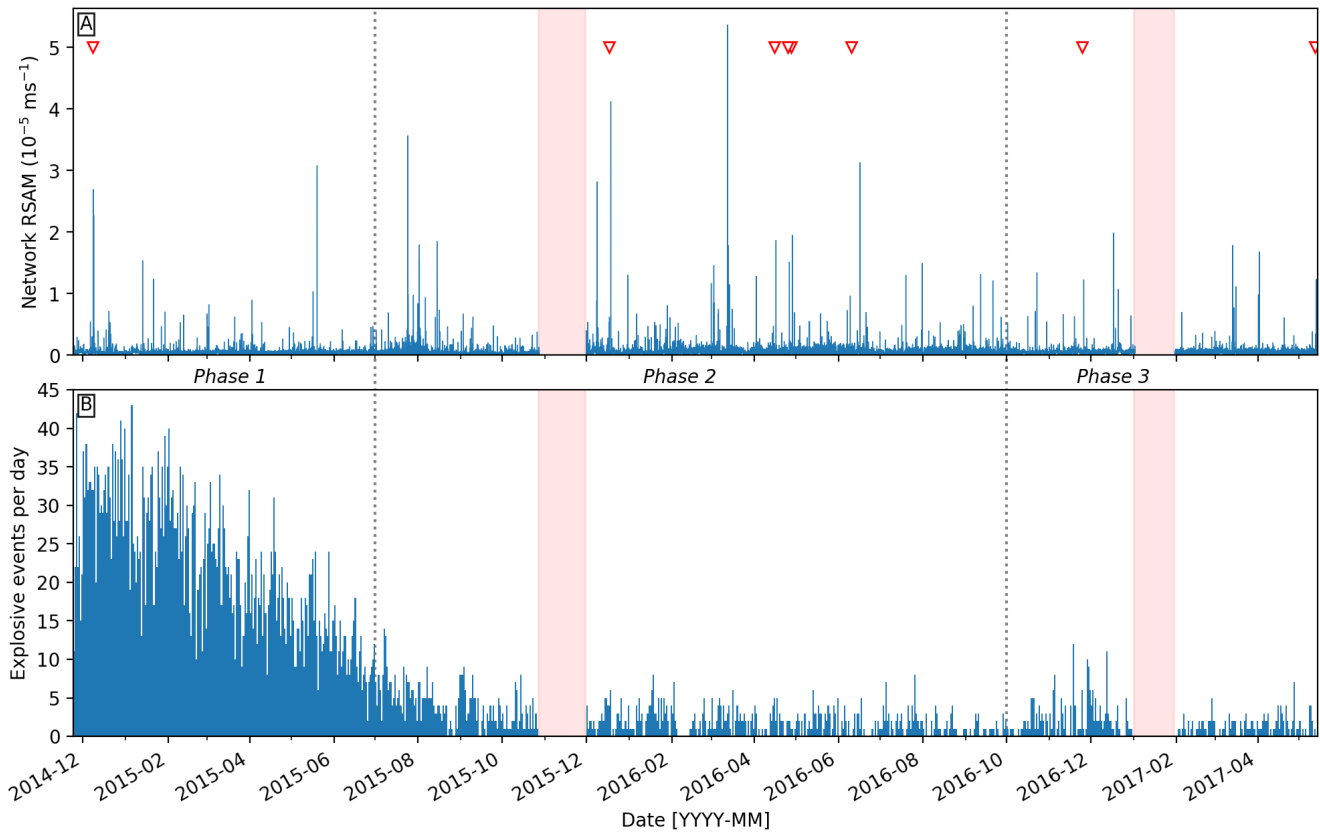


Figure 4. (A) Network real-time seismic amplitude measurement (Network RSAM) between November 2014 and May 2017. Red triangles indicate $M6+$ tectonic earthquakes located within 800 km of Santiaguito. (B) Daily counts of explosive events detected at Santiaguito dome complex over the same time period. Periods shaded in light red indicate when no stations in the network were recording data. Dotted lines delineate the three phases of eruptive activity as described in the text.

243 4.2 Regular low-energy explosions

244 Phase 1 was characterized by regular gas-and-ash plumes at intervals of 0.5-1 h (Fig. 4B). This behavior
 245 had been observed at Santiaguito since 1975 (Rose, 1987) and has been well documented and analyzed
 246 through multiple field studies and methods (Bluth and Rose, 2004; Johnson et al., 2004, 2008; Sahetapy-
 247 Engel et al., 2008; Yamamoto et al., 2008; Johnson et al., 2009; Johnson and Lees, 2010; Sanderson et al.,
 248 2010; Holland et al., 2011; Johnson et al., 2011, 2014; Scharff et al., 2014; Lavallée et al., 2015; De Angelis
 249 et al., 2016). A typical example of the seismic waveform generated by explosions of this magnitude is
 250 presented in Figure 5, along with a thermal image of the same event. Analysis of acoustic and thermal data
 251 recorded during a similar explosion on 30th November 2014 finds that these events contain only minor
 252 fractions of ash, therefore little magma fragmentation is taking place in the conduit (De Angelis et al.,
 253 2016).

254 4.3 Deformation cycles

255 In 2012, the regular low-energy explosions were observed to coincide with a ~ 26 -minute inflation-
 256 deflation cycles of the volcanic edifice, with peak inflation commonly culminating in an outgassing event
 257 or an explosion (Johnson et al., 2014; Lavallée et al., 2015). We tested whether the eruptive activity during
 258 the first few months of our study was similar to that reported by Johnson et al. (2014). Radial tilt can be

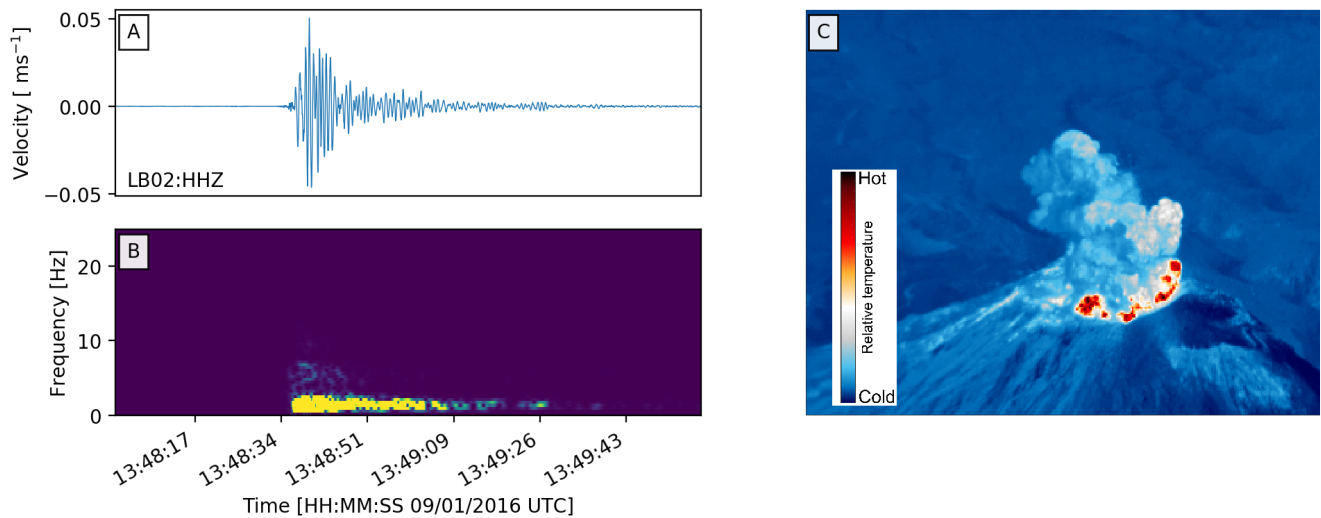


Figure 5. Seismic record (A) and frequency spectrogram (B) of a small explosion recorded on 09/01/2016 at station LB02. A 0.1 Hz high-pass filter has been applied to the seismic record. (C) Thermal image of the explosion event captured at 09/01/2016 13:48:49.456 (UTC), approximately 16 seconds after the explosion plume first appears at the surface.

259 derived from broadband seismic data by a magnification of the low-pass filtered integral of the displacement
 260 time-series (De Angelis and Bodin, 2012). Here, we used data recorded on 1st December 2014 by one of
 261 the closest stations, LB04 (Fig. 1, 6B), located approximately 500 m from the eruptive vent. The calculated
 262 radial tilt (Fig. 6A) display similar cyclic deformation characteristics to those observed in 2012 at the same
 263 location (Fig. 6C,D; Johnson et al., 2014), but with a periodicity of 30-90 minutes. The most pronounced
 264 inflation phase commonly culminate with explosions (marked by more pronounced peaks in Fig. 6B),
 265 whereas smaller inflation phases resulted in outgassing events (Fig. 6A, B). Our observations suggest that
 266 activity observed until June 2015 was a continuation of the eruptive activity that had been characteristic of
 267 El Caliente since 1975.

268 4.4 Large explosions and blast waves

269 Eruptive activity during Phase 2 (July 2015 to September 2016) at Santiaguito was defined by the irregular
 270 occurrence of large explosions, producing ash plumes up to 7 km a.s.l. The most intense eruptions were
 271 reported in the first half of 2016, between February and May (Fig. 2D, Section 3.3). This series of large
 272 explosions caused the excavation of the eruptive vent at the Caliente dome (Fig. 2H). The explosions in early
 273 February 2016 generated powerful blast waves that were heard up to 25 km away from the vent, resulted in
 274 minor damage to nearby buildings, including shattered windows (Section 3.3), and were recorded by the
 275 acoustic microphones deployed around the volcano (Fig. 7).

276 Blast waves (a.k.a. shock waves) are generated by the supersonic release of pressure in a confined small
 277 volume (Needham, 2010). Blast waves generated during volcanic explosions are often observed visually
 278 but are rarely recorded in the acoustic record (Marchetti et al., 2013). The acoustic waveforms generated
 279 during such events are characterized by the sharp compressive onset defined by the leading shock front
 280 and immediately followed by a longer-lasting rarefaction wave of smaller amplitude (Needham, 2010), a
 281 sequence well defined by the Friedlander equation (Section 1.2 in supplementary material; Marchetti et al.,
 282 2013). Indeed, the acoustic waveforms recorded during the explosions at Santiaguito in early February
 283 2016 are well approximated by the Friedlander equation (Fig. 7), indicative of supersonic pressure release

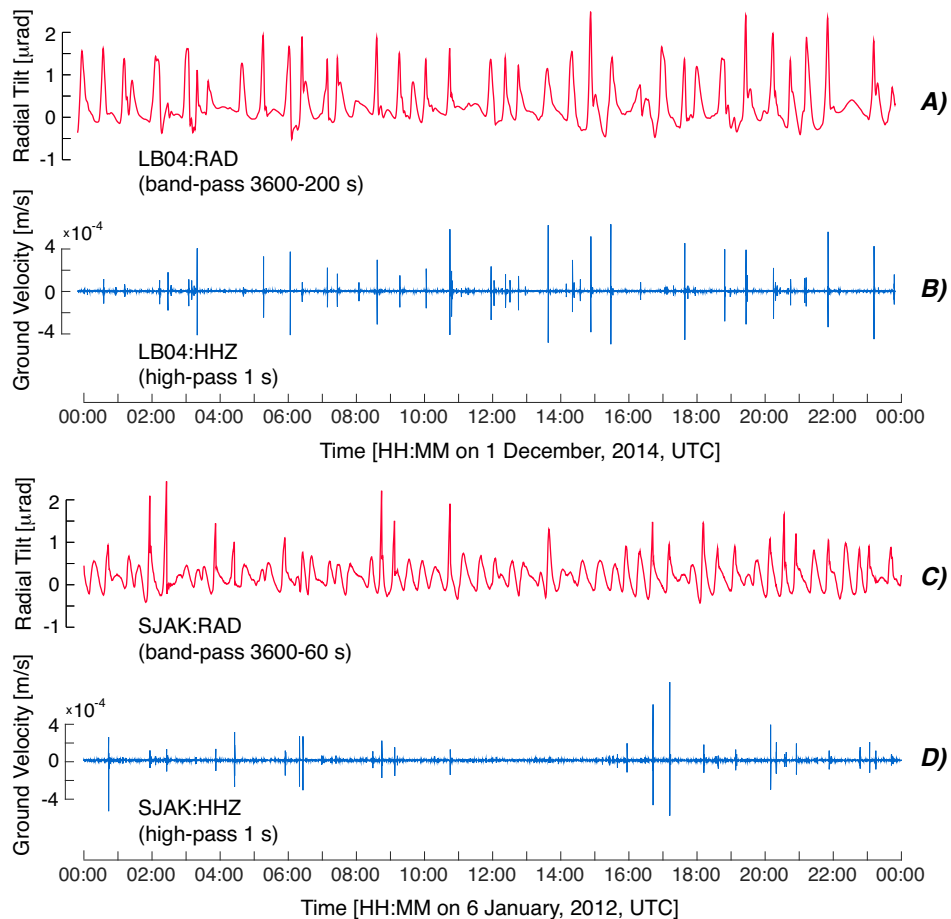


Figure 6. Radial tilt (red) derived from ground velocity (blue) recorded from seismometers or tiltmeters located close to El Caliente vent during two studies: LB04 (A,B) from our study, and SJAK (C,D) from Johnson et al. (2014).

284 at the vent. This represents the first such direct measurement of blast waves at Santiaguito dome complex
 285 (to our knowledge).

286 4.5 Pyroclastic density currents

287 PDCs were often reported on the flanks of Santiaguito during the period of heightened explosive activity
 288 of Phase 2. Large explosions were frequently accompanied by one or multiple PDCs descending the SW, S
 289 or SE flanks of the El Caliente dome with run-out distances of up to 3 km. No significant PDC was reported
 290 without an accompanying explosion. Most PDCs resulted from partial collapse of the eruptive column
 291 during explosive events. One PDC on 8th March 2016 was reported as caused by an additional collapse of
 292 part of the El Caliente dome, triggered by a moderate explosion (Global Volcanism Program, 2016b). It
 293 remains unconfirmed that several PDCs could have been caused by the excavation of the El Caliente vent
 294 during large explosive activity (Section 3.3, Fig. 2H).

295 Multiple PDC events were recorded in our dataset during our period of study. A seismic waveform for
 296 a PDC observed on 19th June 2016 is plotted in Figure 8C. This event, recorded was reported by the
 297 Santiaguito Volcano Observatory (OVSAN) and the accompanying explosion produced a plume up to a
 298 height of 5 km a.s.l. (Global Volcanism Program, 2016a). The PDC waveform has a duration of only a few

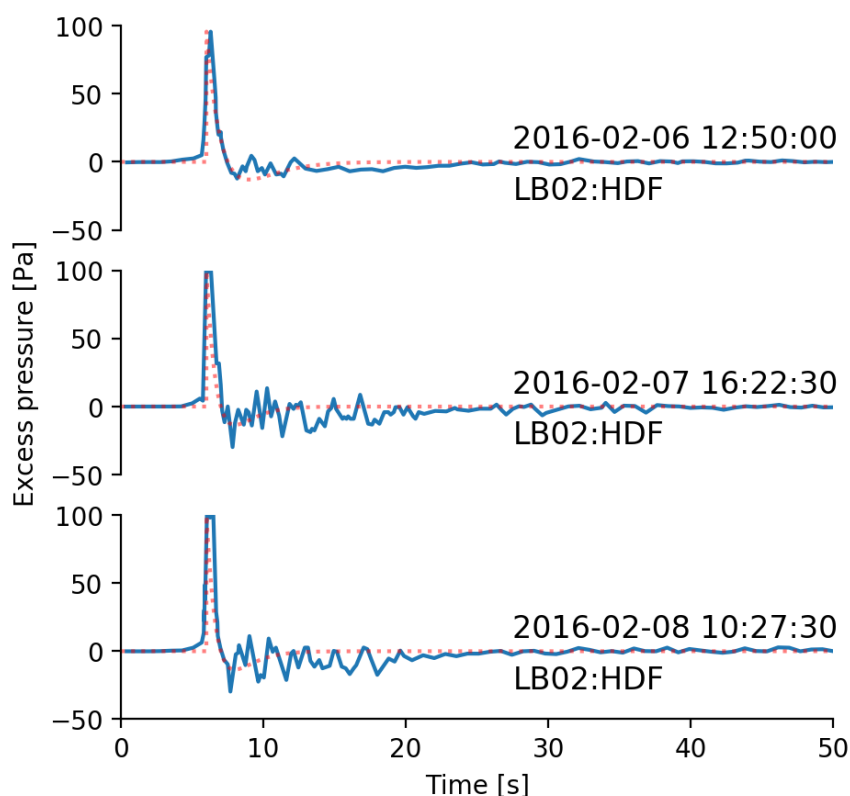


Figure 7. Infrasonic acoustic waveforms (blue line) from three large explosions in early February 2016 as recorded at station LB02. Each event is overlain with the modeled Friedlander wave (red dashed line) that indicates the blast wave nature of the events.

299 minutes, consistent with a relatively short run-out distance down the south or south-western flanks of El
300 Caliente.

301 4.6 Lahars

302 Deposits from PDCs and explosions since May 2014 have provided a large supply of sediment to the
303 fluvial systems around Santiaguito. Mobilization of the volcanic material in the annual rainy season triggers
304 lahars and aggradation. Lahar activity typically impacts a fluvial system extending as much as 60 km SW
305 from Santiaguito to the Pacific coast of Guatemala, a heavily populated and farmed zone (Harris et al.,
306 2006). Here we focus on the largest lahars that occurred during our period of analysis, particularly those
307 reported by INSIVUMEH and the Bulletin of the Global Volcanism Network, published on the Global
308 Volcanism Program website (volcano.si.edu). Smaller, unreported lahars will be difficult to distinguish
309 from PDCs without additional information, since both types of events share similar frequency content and
310 amplitudes (e.g. Fig. 8; Huang et al., 2007).

311 Between November 2014 and May 2017, at least 16 major lahars were observed and reported descending
312 the barrancas (steep-sided valleys). In the seismic record, these events were characterized by emergent
313 waveforms with durations of up to one hour (Fig. 8A). The energy in the lahar signals were broadly
314 distributed below 25 Hz, but the majority was concentrated below 10 Hz (Fig. 8B). Six major barrancas
315 lie between stations LB01 and LS04 (Fig. 1), and it is difficult to assess within which of these the lahars
316 traveled based on the available seismic and acoustic data.

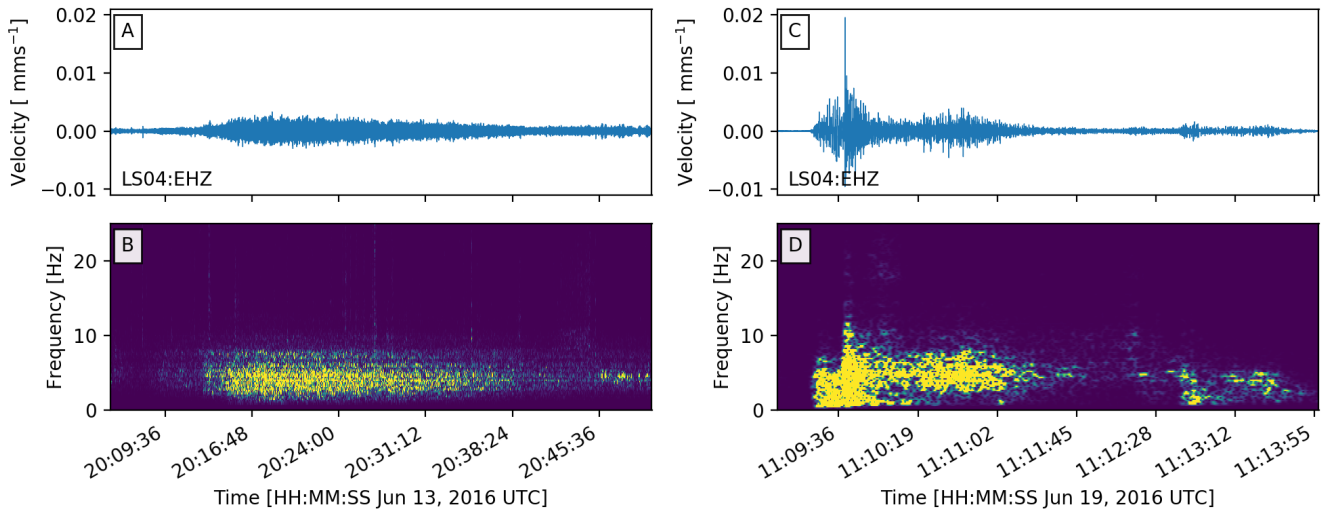


Figure 8. Example Seismic records (A,C) and frequency spectrograms (B, D) of a Lahar on 13th June 2016 (A,B) and an explosion followed by a pyroclastic density current on 19th June 2016 (C,D). The unfiltered seismic waveforms were recorded at station LS04. The waveform and frequency characteristics shown here are typical for these types of events as recorded at this station.

317 4.7 Rockfalls

318 Rockfall were frequently recorded throughout our period of study. Three sources of rockfall were
 319 identified around Santiaguito during field campaigns. The first, and the source of a clear majority of
 320 rockfalls in our dataset, was the unstable scarp formed on the southwestern flank of Santa Maria volcano
 321 during the 1902 eruption (Williams and Self, 1983). Rockfalls were also observed along the flanks of
 322 the El Caliente (Fig. 9, Movie S1) and La Mitad lava domes, an indication of their instability. Rockfalls
 323 originated on the southwestern flank of Santa Maria could be easily identified by their seismic amplitude
 324 distribution across the network (larger amplitude waveforms were recorded at station LS06 for rockfalls
 325 from the unstable scarp) and by visual observations in the field. On inspection of the seismic data, the
 326 number of rockfalls inferred to have originated from the lava domes showed no obvious correlation with
 327 the number and energy of explosive events during the study period. Small and infrequent rockfalls from the
 328 front and flank of the 2014 lava flow were also witnessed but rarely recorded.

329 4.8 Volcano-tectonic swarms

330 Volcano-tectonic (VT) earthquakes are characterized by sharp, mostly impulsive onsets of P- and S-waves
 331 with broad spectra up to 15 Hz (Lahr et al., 1994). They share similarities with tectonic earthquakes, but
 332 are instead interpreted as the result of stress perturbation due to magmatic intrusion (e.g. Sigmundsson
 333 et al., 2015) or by hydrothermal fluids expelled from a magmatic body (e.g. Hill, 1996). Rather than
 334 mainshock-aftershock sequences that define major tectonic earthquakes, VTs often occur as intense swarms
 335 of earthquakes located beneath or near a volcano. Here, we report the first evidence of VT swarm activity
 336 recorded at Santiaguito volcano (to our knowledge).

337 Several VT swarms were detected during mid-2016. Figure 10 shows seismic data for a swarm recorded
 338 on the 24th July 2016. The swarm started at approximately 00:00 (UTC) and continued for a total of
 339 approximately 11 hours. During that time, 275 VT earthquakes were recorded at station LB03. The
 340 average repose interval between individual earthquakes throughout the swarm decreased from 600 to 120

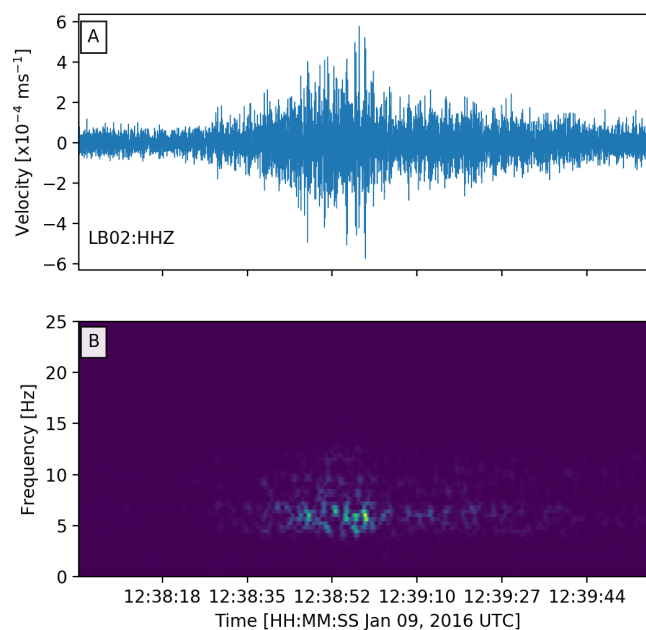


Figure 9. Seismic record (A) and frequency spectrogram (B) of rockfall recorded at station LB02 on 9th January 2016. A high-pass filter at 0.5 Hz has been applied to the seismic record. The source location for this event was down the western flank of Caliente dome. A thermal recording of the event can be seen in Movie S1.

341 s. Concurrently, their amplitudes slowly increased through the swarm. Waveform correlation analysis of
 342 the events suggests there is very little degree of repetitiveness throughout the swarm, suggesting no VTs
 343 repeatedly occurred in the same location. The swarm ended concurrently with a relatively minor explosion,
 344 although it is unclear if the two events are related. No other explosions were observed to be preceded by
 345 VT events.

5 CONCLUDING REMARKS

346 The progression in explosive activity at Santiaguito from 2014 to 2017 has been recorded in detail by the
 347 seismic and infrasound dataset, complemented by detailed optical and thermal observations made during
 348 field campaigns. The regular explosive activity seen in the first phase of our dataset appears to be a clear
 349 continuation of that reported at Santiaguito by previous studies (Sahetapy-Engel et al., 2008; Johnson
 350 et al., 2014). The first indication for a change in explosive behavior occurred when the first large vulcanian
 351 explosions occurred in late 2015. However, it is clear from the explosion database compiled here that the
 352 transition between eruptive styles took place gradually over the latter half of 2015 (Fig. 4B). This raises the
 353 question of what process had occurred within the volcanic system that promoted this transition in activity.

354 Similar escalations in activity have been observed at other long-term silicic effusive eruptions, including
 355 Volcán de Colima (Mexico) and Soufrière Hills volcano (Montserrat). Cyclic effusive activity at Volcán
 356 de Colima from 1998 to 2017 was interrupted by heightened explosive activity in 2005 and 2015. The
 357 high pressures needed to produce the vulcanian explosions in 2005 were explained by strong vertical
 358 gradients in viscosity within the magma column as well as the growth of microlites in the upper conduit
 359 (Arámbula-Mendoza et al., 2011). The rapid transition to dome collapse and explosive activity in 2015
 360 was linked to the arrival of a batch of relatively volatile-rich magma into the shallow magma column

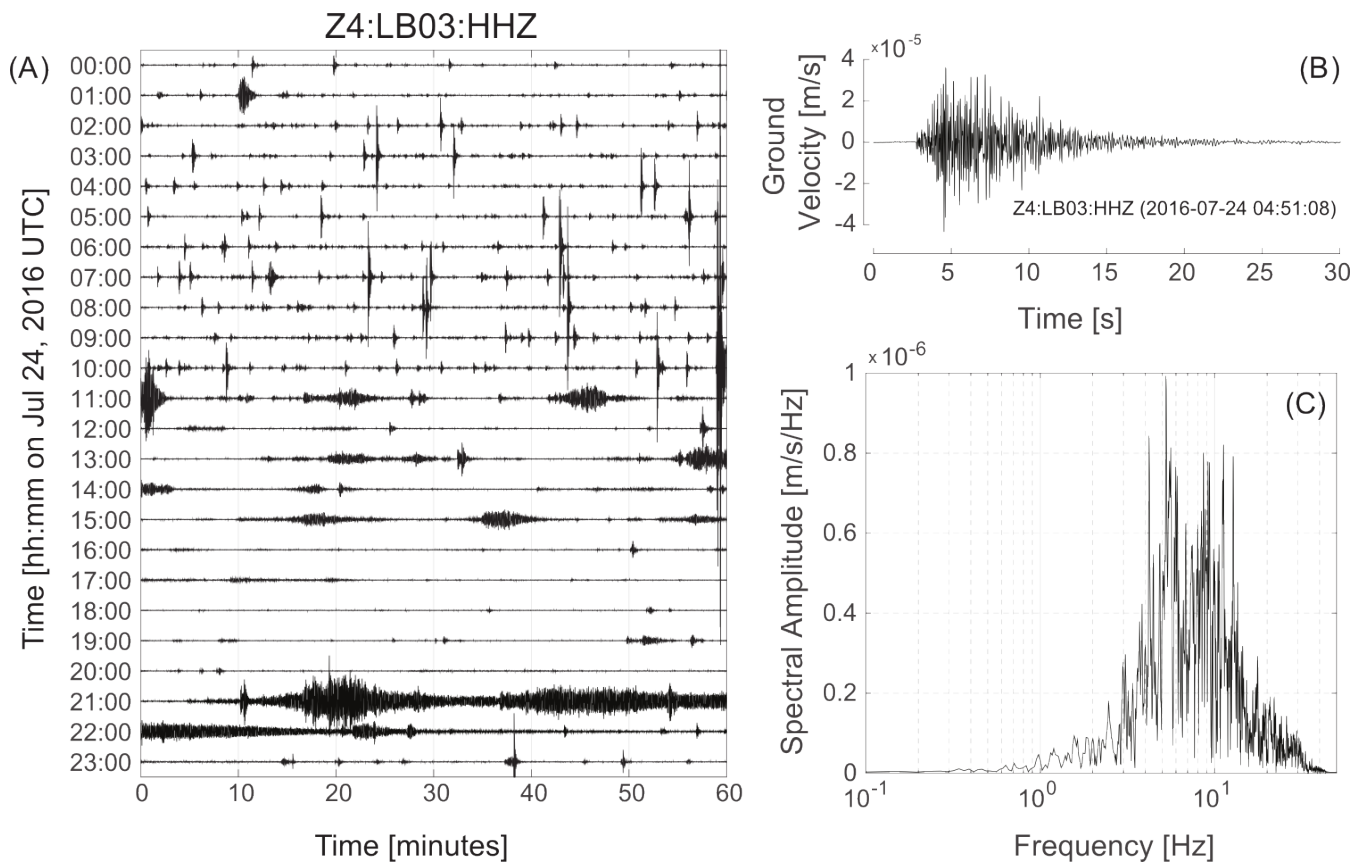


Figure 10. (A) 24-hour helicorder from station LB03 on 24th July 2017 showing a short swarm of volcano-tectonic earthquakes from 00:00 to 11:00 UTC, followed closely by an explosive event. The long-lived high amplitude event from 21:00 to 22:30 is likely an unreported lahar. (B) A waveform and its frequency spectrum (C) of one volcano-tectonic earthquake during the swarm in (A), demonstrating the high-frequency nature of the volcano-tectonic events.

361 (Reyes-Dávila et al., 2016). Soufrière Hills volcano underwent multiple phases of effusive and explosive
 362 activity between 1995 and 2010 (Wadge et al., 2014). Christopher et al. (2015) proposed the presence
 363 of a multi-level, mature magmatic system beneath the volcano and theorized that destabilization of the
 364 system can lead to elevated levels of volcanic activity at the surface. Destabilization may be caused by
 365 mixing of fluid-rich and crystal-rich magmas which led to degassing and pressurization of the system. At
 366 Santiaguito, the 2015-2016 escalation in activity was preceded by a long-term decay in extrusion rates
 367 since 1922 (Harris et al., 2003) and a decrease in the bulk SiO₂ content of the eruptive products (Scott
 368 et al., 2013), suggesting a magmatic system becoming increasingly depleted of eruptible magma. It is also
 369 worth noting that this period of escalated activity followed a short period of relatively heightened effusion
 370 rates, manifested by three lava flows since 2010 (Rhodes et al., 2018, ; Hornby et al. *in prep*). Further
 371 work is needed, particularly with geochemical analyses of the eruptive products, before conclusions can be
 372 drawn regarding the trigger mechanism for escalated eruptive activity at Santiaguito.

373 The preliminary overview of the activity and our observations presented here represent the foundations
 374 for future studies and show the value of investment in long-term multiparametric monitoring of active
 375 volcanoes. A detailed study into the trigger mechanisms of the large vulcanian explosions in 2015 can lead
 376 to improved near-real time emergency responses (e.g. Arámbula-Mendoza et al., 2011) as well as more
 377 accurate ash-tracking systems, an important tool for the aviation industry (e.g. Mastin et al., 2009). Detailed

378 analysis of the seismic and infrasonic signals generated during lahars or PDCs, combined with studies of
379 their physical characteristics, could produce improved hazard assessments (e.g. Johnson and Palma, 2015).
380 Locating and tracking the evolution of the volcano-tectonic seismic swarms in mid-2016 may give useful
381 insights into the short- and long-term behavior of Santiaguito, particularly with regards to the transition
382 from explosive to effusive activity in late 2016 (e.g. White and McCausland, 2016). Complementary
383 insights may also be gained from studies carried out on the geochemical and rheological properties of the
384 recent eruptive products (e.g. Rhodes et al., 2018), changes in the morphology of the dome in relation
385 to eruptive activity (e.g. James and Varley, 2012) as well from the thermal and optical images of the
386 explosions collected during field campaigns (e.g. Sahetapy-Engel et al., 2008).

AUTHOR CONTRIBUTIONS

387 OL, AL, ADM, SDA, AH, FvA, JK, AR, GC and YL conducted fieldwork around Santiaguito across
388 multiple field campaigns from 2014 to 2017. OL, ADM, SDA, and IA processed all the seismic and
389 infrasound data, while AL and JK processed and analysed the thermal images. OL compiled all the data
390 and wrote the manuscript, to which all authors have contributed.

FUNDING

391 YL, OL, AL, AH, FvA and JK acknowledge support from the European Research Council Starting Grant on
392 Strain Localisation in Magma (SLiM, 306488). SDA, AR and YL thank the Natural Environment Research
393 Council (NERC) for an urgency grant on “Rapid deployment of a multi-parameter geophysical experiment
394 at Santiaguito volcano, Guatemala, following a marked increase in explosive activity” (NE/P007708/1) and
395 the Liverpool Earth Observatory for financially supporting the undertaking of this long-term, large-scale,
396 multi-parametric investigation. ADM was partially funded by NERC grant NE/P00105X/1 and the Spanish
397 Mineco Project KNOWAVES (TEC2015-68752). IA was supported by Spanish research grant MECD Jose
398 Castillejo CAS17/00154.

ACKNOWLEDGMENTS

399 The authors acknowledge the support provided by the Instituto Nacional de Sismología, Vulcanología,
400 Meteorología, e Hidrología (INSIVUMEH), Guatemala, and the staff of the Observatorio Vulcanológico
401 Santiaguito (OVSAN). We are also grateful to our local guide and network manager in Guatemala, A.
402 Pineda, as well as to J. Johnson for permission to use the data presented in Fig. 6C, D. The raw data
403 supporting the conclusions of this manuscript will be made available by the authors, without undue
404 reservation, to any qualified researcher.

REFERENCES

- 405 Arámbula-Mendoza, R., Lesage, P., Valdés-González, C., Varley, N. R., Reyes-Dávila, G. A., and Navarro,
406 C. (2011). Seismic activity that accompanied the effusive and explosive eruptions during the 2004-2005
407 period at Volcán de Colima, Mexico. *Journal of Volcanology and Geothermal Research* 205, 30–46.
408 doi:10.1016/j.jvolgeores.2011.02.009
- 409 Bluth, G. J. and Rose, W. I. (2004). Observations of eruptive activity at Santiaguito volcano, Guatemala.
410 *Journal of Volcanology and Geothermal Research* 136, 297–302. doi:10.1016/j.jvolgeores.2004.06.001

- 411 Calder, E. S., Lavallée, Y., Kendrick, J. E., and Bernstein, M. (2015). Lava Dome Eruptions. In *The*
412 *Encyclopedia of Volcanoes 2nd Edition*, eds. H. Sigurdsson, B. Houghton, H. Rymer, J. Stix, and S. R.
413 McNutt. 343–362
- 414 Christopher, T. E., Blundy, J., Cashman, K., Cole, P. D., Edmonds, M., Smith, P. J., et al. (2015).
415 Crustal-scale degassing due to magma system destabilization and magma-gas decoupling at Soufrière
416 Hills Volcano, Montserrat. *Geochemistry Geophysics Geosystems* 16, 2797–2811. doi:10.1002/
417 2015GC005791
- 418 De Angelis, S. and Bodin, P. (2012). Watching the Wind: Seismic Data Contamination at Long Periods
419 due to Atmospheric Pressure-Field-Induced Tilting. *Bulletin of the Seismological Society of America*
420 102, 1255–1265. doi:10.1785/0120110186
- 421 De Angelis, S., Lamb, O. D., Lamur, A. N., Hornby, A. J., von Aulock, F. W., Chigna, G., et al. (2016).
422 Characterization of moderate ash-and-gas explosions at Santiaguito volcano, Guatemala, from infrasound
423 waveform inversion and thermal infrared. *Geophysical Research Letters* 43. doi:10.1002/2016GL069098
- 424 Delle Donne, D. and Ripepe, M. (2012). High-frame rate thermal imagery of Strombolian explosions:
425 Implications for explosive and infrasonic source dynamics. *Journal of Geophysical Research* 117.
426 doi:10.1029/2011JB008987
- 427 Dingwell, D. B. (1996). Volcanic Dilemma: Flow or Blow? *Science* 273, 1054–1055
- 428 Edmonds, M., Oppenheimer, C., Pyle, D. M., Herd, R. A., and Thompson, G. (2003). SO₂ emissions
429 from Soufriere Hills Volcano and their relationship to conduit permeability, hydrothermal interaction
430 and degassing regime. *Journal of Volcanology and Geothermal Research* 124, 23–43
- 431 Endo, E. T. and Murray, T. (1991). Real-time Seismic Amplitude Measurement (RSAM): a volcano
432 monitoring and prediction tool. *Bulletin of Volcanology* 53, 533–545
- 433 Farquharson, J. I., Heap, M. J., Varley, N. R., Baud, P., and Reuschlé, T. (2015). Permeability and
434 porosity relationships of edifice-forming andesites: A combined field and laboratory study. *Journal of*
435 *Volcanology and Geothermal Research* 297, 52–68. doi:10.1016/j.jvolgeores.2015.03.016
- 436 Fink, J. H. (1990). *Lava Flows and Domes*, vol. 2 of *IAVCEI Proceedings in Volcanology* (Berlin,
437 Heidelberg: Springer Berlin Heidelberg). doi:10.1007/978-3-642-74379-5
- 438 Gaunt, H., Sammonds, P. R., Meredith, P. G., Smith, R., and Pallister, J. S. (2014). Pathways for
439 degassing during the lava dome eruption of Mount St. Helens 2004–2008. *Geology* 42, 947–950.
440 doi:10.1130/G35940.1
- 441 Global Volcanism Program (2015). Report on Santa Maria (Guatemala) — July 2015. In *Bulletin of the*
442 *Global Volcanism Network*, ed. E. Venzke (Smithsonian Institution Press), vol. 40
- 443 Global Volcanism Program (2016a). Report on Santa Maria (Guatemala) — February 2016. In *Bulletin of*
444 *the Global Volcanism Network*, ed. E. Venzke (Smithsonian Institution Press), vol. 41
- 445 Global Volcanism Program (2016b). Report on Santa Maria (Guatemala) — September 2016. In *Bulletin*
446 *of the Global Volcanism Network*, ed. E. Venzke (Smithsonian Institution Press), vol. 41
- 447 Global Volcanism Program (2017). Report on Santa Maria (Guatemala) — December 2017. In *Bulletin*
448 *of the Global Volcanism Network*, ed. E. Venzke (Smithsonian Institution Press), vol. 42
- 449 Gonnermann, H. M. and Manga, M. (2007). The Fluid Mechanics Inside a Volcano. *Annual Review of*
450 *Fluid Mechanics* 39, 321–356. doi:10.1146/annurev.fluid.39.050905.110207
- 451 Goto, A. (1999). A new model for volcanic earthquake at Unzen Volcano: Melt Rupture Model. *Geophysical*
452 *Research Letters* 26, 2541–2544. doi:10.1029/1999GL900569
- 453 Harris, A. J. L., Rose, W. I., and Flynn, L. P. (2003). Temporal trends in lava dome extrusion at Santiaguito
454 1922 – 2000. *Bulletin of Volcanology* 65, 77–89. doi:10.1007/s00445-002-0243-0

- 455 Harris, A. J. L., Vallance, J. W., Kimberly, P., Rose, W. I., Matías, O., Bunzendahl, E., et al. (2006).
456 Downstream aggradation owing to lava dome extrusion and rainfall runoff at Volcán Santiaguigo,
457 Guatemala. *Geological Society of America Special Paper* 412, 85–104. doi:10.1130/2006.2412(05).
- 458 Heap, M. J., Farquharson, J. I., Baud, P., Lavallée, Y., and Reuschlé, T. (2015a). Fracture and compaction
459 of andesite in a volcanic edifice. *Bulletin of Volcanology* 77. doi:10.1007/s00445-015-0938-7
- 460 Heap, M. J., Xu, T., Kushnir, A. R., Kennedy, B. M., and Chen, C.-f. (2015b). Fracture of magma
461 containing overpressurised pores. *Journal of Volcanology and Geothermal Research* 301, 180–190.
462 doi:10.1016/j.jvolgeores.2015.05.016
- 463 Hill, D. P. (1996). Earthquakes and Carbon Dioxide beneath Mammoth Mountain, California. *Seismological*
464 *Research Letters* 67, 8–15
- 465 Holland, A. P., Watson, I., Phillips, J. C., Caricchi, L., and Dalton, M. P. (2011). Degassing processes
466 during lava dome growth: Insights from Santiaguigo lava dome, Guatemala. *Journal of Volcanology and*
467 *Geothermal Research* 202, 153–166. doi:10.1016/j.jvolgeores.2011.02.004
- 468 Huang, C.-J., Yin, H.-Y., Chen, C.-Y., Yeh, C.-H., and Wang, C.-L. (2007). Ground vibrations produced
469 by rock motions and debris flows. *Journal of Geophysical Research: Earth Surface* 112. doi:10.1029/
470 2005JF000437
- 471 Iverson, R. M., Dzurisin, D., Gardner, C. A., Gerlach, T. M., LaHusen, R. G., Lisowski, M., et al. (2006).
472 Dynamics of seismogenic volcanic extrusion at Mount St Helens in 2004–05. *Nature* 444, 439–43.
473 doi:10.1038/nature05322
- 474 James, M. R. and Varley, N. (2012). Identification of structural controls in an active lava dome with
475 high resolution DEMs: Volcán de Colima, Mexico. *Geophysical Research Letters* 39. doi:10.1029/
476 2012GL054245
- 477 Johnson, J. B., Harris, A. J. L., Sahetapy-Engel, S. T. M., Wolf, R., and Rose, W. I. (2004). Explosion
478 dynamics of pyroclastic eruptions at Santiaguigo Volcano. *Geophysical Research Letters* 31, L06610.
479 doi:10.1029/2003GL019079
- 480 Johnson, J. B. and Lees, J. M. (2010). Sound produced by the rapidly inflating Santiaguigo lava dome,
481 Guatemala. *Geophysical Research Letters* 37, 1–6. doi:10.1029/2010GL045217
- 482 Johnson, J. B., Lees, J. M., Gerst, A., Sahagian, D., and Varley, N. R. (2008). Long-period earthquakes and
483 co-eruptive dome inflation seen with particle image velocimetry. *Nature* 456, 377–381. doi:10.1038/
484 nature07429
- 485 Johnson, J. B., Lees, J. M., and Gordeev, E. I. (1998). Degassing explosions at Karymsky Volcano,
486 Kamchatka. *Geophysical Research Letters* 25, 3999–4002. doi:10.1029/1998GL900102
- 487 Johnson, J. B., Lees, J. M., and Varley, N. R. (2011). Characterizing complex eruptive activity at Santiaguigo,
488 Guatemala using infrasound semblance in networked arrays. *Journal of Volcanology and Geothermal*
489 *Research* 199, 1–14. doi:10.1016/j.jvolgeores.2010.08.005
- 490 Johnson, J. B., Lyons, J. J., Andrews, B. J., and Lees, J. M. (2014). Explosive dome eruptions modulated
491 by periodic gas-driven inflation. *Geophysical Research Letters* 41. doi:10.1002/2014GL061310
- 492 Johnson, J. B. and Palma, J. L. (2015). Lahar infrasound associated with Villarrica’s March 3, 2015
493 eruption. *Geophysical Research Letters* 42, 6324–6331. doi:10.1002/2015GL065024
- 494 Johnson, J. B., Sanderson, R., Lyons, J. J., Escobar-Wolf, R., Waite, G. P., and Lees, J. M. (2009).
495 Dissection of a composite volcanic earthquake at Santiaguigo, Guatemala. *Geophysical Research Letters*
496 36, L16308. doi:10.1029/2009GL039370
- 497 Jones, K. and Johnson, J. B. (2011). Mapping complex vent eruptive activity at Santiaguigo, Guatemala
498 using network infrasound semblance. *Journal of Volcanology and Geothermal Research* 199, 15–24.
499 doi:10.1016/j.jvolgeores.2010.08.006

- 500 Kendrick, J. E., Lavallée, Y., Varley, N. R., Wadsworth, F. B., Lamb, O. D., and Vasseur, J. (2016). Blowing
501 Off Steam: Tuffisite Formation As a Regulator for Lava Dome Eruptions. *Frontiers in Earth Science* 4.
502 doi:10.3389/feart.2016.00041
- 503 Kim, K. and Lees, J. M. (2015). Imaging volcanic infrasound sources using time reversal mirror algorithm.
504 *Geophysical Journal International* 202, 1663–1676. doi:10.1093/gji/ggv237
- 505 Lahr, J. C., Chouet, B. A., Stephens, C. D., Power, J. A., and Page, R. A. (1994). Earthquake classification,
506 location, and error analysis in a volcanic environment: implications for the magmatic system of the
507 1989–1990 eruptions at Redoubt Volcano, Alaska. *Journal of Volcanology and Geothermal Research* 62,
508 137–151
- 509 Lamb, O. D., De Angelis, S., Umakoshi, K., Hornby, A. J., Kendrick, J. E., and Lavallée, Y. (2015).
510 Repetitive fracturing during spine extrusion at Unzen volcano, Japan. *Solid Earth* 6, 1277–1293.
511 doi:10.5194/se-6-1277-2015
- 512 Lavallée, Y., Benson, P. M., Heap, M. J., Hess, K.-U., Flaws, A., Schillinger, B., et al. (2013).
513 Reconstructing magma failure and the degassing network of dome-building eruptions. *Geology* 41,
514 515–518. doi:10.1130/G33948.1
- 515 Lavallée, Y., Dingwell, D. B., Johnson, J. B., Cimorelli, C., Hornby, A. J., Kendrick, J. E., et al. (2015).
516 Thermal vesiculation during volcanic eruptions. *Nature* 528, 544–547. doi:10.1038/nature16153
- 517 Lavallée, Y., Meredith, P. G., Dingwell, D. B., Hess, K.-U., Wassermann, J., Cordonnier, B., et al. (2008).
518 Seismogenic lavas and explosive eruption forecasting. *Nature* 453, 507–10. doi:10.1038/nature06980
- 519 Marchetti, E., Ripepe, M., Delle Donne, D., Genco, R., Finizola, A., and Garaebiti, E. (2013). Blast waves
520 from violent explosive activity at Yasur Volcano, Vanuatu. *Geophysical Research Letters* 40, 5838–5843.
521 doi:10.1002/2013GL057900
- 522 Mastin, L. G., Guffanti, M., Servranckx, R., Webley, P. W., Barsotti, S., Dean, K. G., et al. (2009). A
523 multidisciplinary effort to assign realistic source parameters to models of volcanic ash-cloud transport
524 and dispersion during eruptions. *Journal of Volcanology and Geothermal Research* 186, 10–21. doi:10.
525 1016/j.jvolgeores.2009.01.008
- 526 Michaut, C., Ricard, Y., Bercovici, D., and Sparks, R. S. J. (2013). Eruption cyclicality at silicic volcanoes
527 potentially caused by magmatic gas waves. *Nature Geoscience* 6, 856–861. doi:10.1038/ngeo1928
- 528 Needham, C. (2010). *Blast Waves* (Heidelberg: Springer)
- 529 Neuberg, J. W. (2000). Characteristics and causes of shallow seismicity in andesite volcanoes. *Philosophical*
530 *transactions of the Royal Society A* 358, 1533–1546
- 531 Neuberg, J. W., Tuffen, H., Collier, L., Green, D. N., Powell, T., and Dingwell, D. B. (2006). The trigger
532 mechanism of low-frequency earthquakes on Montserrat. *Journal of Volcanology and Geothermal*
533 *Research* 153, 37–50. doi:10.1016/j.jvolgeores.2005.08.008
- 534 Papale, P. (1999). Strain-induced magma fragmentation in explosive eruptions. *Nature* 397, 425–428.
535 doi:10.1038/17109
- 536 Reyes-Dávila, G. A., Arámbula-Mendoza, R., Espinasa-Pereña, R., Pankhurst, M. J., Navarro-Ochoa, C.,
537 Savov, I. P., et al. (2016). Volcán de Colima dome collapse of July, 2015 and associated pyroclastic
538 density currents. *Journal of Volcanology and Geothermal Research* 320, 100–106. doi:10.1016/j.
539 jvolgeores.2016.04.015
- 540 Rhodes, E., Kennedy, B. M., Lavallée, Y., Hornby, A., Edwards, M., and Chigna, G. (2018). Textural
541 Insights Into the Evolving Lava Dome Cycles at Santiaguito Lava Dome, Guatemala. *Frontiers in Earth*
542 *Science* 6, 30. doi:10.3389/feart.2018.00030
- 543 Rose, W. I. (1973). Pattern and mechanism of volcanic activity at the Santiaguito Volcanic Dome,
544 Guatemala. *Bulletin Volcanologique* 37, 73–94. doi:10.1007/BF02596881

- 545 Rose, W. I. (1987). Volcanic activity at Santiaguito Volcano 1976-1984. *Geological Society of America*
546 *Special Paper 212*, 17–27doi:10.1130/SPE212-p17
- 547 Sahetapy-Engel, S. T. M., Harris, A. J. L., and Marchetti, E. (2008). Thermal, seismic and infrasound
548 observations of persistent explosive activity and conduit dynamics at Santiaguito lava dome, Guatemala.
549 *Journal of Volcanology and Geothermal Research* 173, 1–14. doi:10.1016/j.jvolgeores.2007.11.026
- 550 Sanderson, R., Johnson, J. B., and Lees, J. M. (2010). Ultra-long period seismic signals and cyclic deflation
551 coincident with eruptions at Santiaguito volcano, Guatemala. *Journal of Volcanology and Geothermal*
552 *Research* 198, 35–44. doi:10.1016/j.jvolgeores.2010.08.007
- 553 Scharff, L., Hort, M., and Gerst, A. (2014). The dynamics of the dome at Santiaguito volcano, Guatemala.
554 *Geophysical Journal International* 197, 926–942. doi:10.1093/gji/ggu069
- 555 Scheu, B., Kueppers, U., Mueller, S., Spieler, O., and Dingwell, D. B. (2008). Experimental volcanology
556 on eruptive products of Unzen volcano. *Journal of Volcanology and Geothermal Research* 175, 110–119.
557 doi:10.1016/j.jvolgeores.2008.03.023
- 558 Scott, J. A., Pyle, D. M., Mather, T. A., and Rose, W. I. (2013). Geochemistry and evolution of the
559 Santiaguito volcanic dome complex, Guatemala. *Journal of Volcanology and Geothermal Research* 252,
560 92–107. doi:10.1016/j.jvolgeores.2012.11.011
- 561 Sigmundsson, F., Hooper, A., Hreinsdóttir, S., Vogfjörð, K. S., Ófeigsson, B. G., Heimisson, E. R., et al.
562 (2015). Segmented lateral dyke growth in a rifting event at Bárðarbunga volcanic system, Iceland.
563 *Nature* 517, 15. doi:10.1038/nature14111
- 564 Sparks, R. S. J. (1997). Causes and consequences of pressurisation in lava dome eruptions. *Earth and*
565 *Planetary Science Letters* 150, 177–189. doi:10.1016/S0012-821X(97)00109-X
- 566 Surono, Jousset, P., Pallister, J., Boichu, M., Buongiorno, M. F., Budisantoso, A., et al. (2012). The
567 2010 explosive eruption of java’s merapi volcano—a ‘100-year’ event. *Journal of Volcanology and*
568 *Geothermal Research* 241-242, 121 – 135. doi:10.1016/j.jvolgeores.2012.06.018
- 569 Wadge, G., Robertson, R. E. A., and Voight, B. (2014). The Eruption of Soufrière Hills Volcano, Montserrat
570 from 2000 to 2010. *Geological Society, London, Memoirs* 39
- 571 White, R. and McCausland, W. (2016). Volcano-tectonic earthquakes: A new tool for estimating intrusive
572 volumes and forecasting eruptions. *Journal of Volcanology and Geothermal Research* 309, 139–155.
573 doi:10.1016/j.jvolgeores.2015.10.020
- 574 Williams, S. N. and Self, S. (1983). The October 1902 plinian eruption of Santa Maria volcano, Guatemala.
575 *Journal of Volcanology and Geothermal Research* 16, 33–56
- 576 Yamamoto, H., Watson, I., Phillips, J. C., and Bluth, G. J. (2008). Rise dynamics and relative ash
577 distribution in vulcanian eruption plumes at Santiaguito Volcano, Guatemala, revealed using an ultraviolet
578 imaging camera. *Geophysical Research Letters* 35, 1–5. doi:10.1029/2007GL032008